HIGH-ORDER FINITE ELEMENT METHOD FOR PLASMA MODELING*

U. Shumlak, R. Lilly, S. Miller, N. Reddell, E. Sousa
Aerospace and Energetics Research Program
University of Washington, Seattle, USA, 98195-2250
Email: shumlak@u.washington.edu

***Abstract*—High-order accurate finite element methods provide unique benefits for problems that have strong anisotropies and complicated geometries and for stiff equation systems that are coupled through large source terms, e.g. Lorentz force, collisions, or atomic reactions. Magnetized plasma simulations of realistic devices using the kinetic or the multi-fluid plasma models are examples that benefit from high-order accuracy. The multi-fluid plasma model only assumes local thermodynamic equilibrium within each fluid, e.g. ion and electron fluids for the two-fluid plasma model. The algorithm implements a discontinuous Galerkin method with an approximate Riemann solver to compute the fluxes of the fluids and electromagnetic fields at the computational cell interfaces. The multi-fluid plasma model has time scales on the order of the electron and ion cyclotron frequencies, the electron and ion plasma frequencies, the electron and ion sound speeds, and the speed of light. A general model for atomic reactions has been developed and is incorporated in the multi-fluid plasma model. The multi-fluid plasma algorithm is implemented in a flexible code framework (WARPX) that allows easy extension of the physical model to include multiple fluids and additional physics. The code runs on multi-processor machines and is being adapted with OpenCL to many-core systems, characteristic of the next generation of high performance computers. The algorithm is applicable to study advanced physics calculations of plasma dynamics including magnetic plasma confinement and astrophysical plasmas. The discontinuous Galerkin method has also been applied to solve the Vlasov-Poisson kinetic model. Recently, a blended finite element algorithm has been developed and implemented which exploits the expected physical behavior to apply either a discontinuous or continuous finite element representation, which improves computational efficiency without sacrificing accuracy.**

I. Introduction

Owing to the complexity of plasma phenomena, a thorough understanding requires validated physical models, verified computational simulations, and well-diagnosed experiments. This paper focuses on developing computational methods for plasma models with sufficient physical and numerical fidelity to generate insight and predictability.

II. Continuum Plasma Models

Discrete models that account for each constituent particle is not particularly useful for the numerical treatment of realistic plasmas where the number of particles (N) and the number of interactions ($> N^2$) is not computationally tractable. Instead an ensemble average is performed to give a statistical description. Plasmas may be most accurately modeled using kinetic theory, where distribution functions, $f_s(\mathbf{x}, \mathbf{v}, t)$, are governed by a Boltzmann equation

$$\frac{\partial f_s}{\partial t} + \mathbf{v} \cdot \frac{\partial f_s}{\partial \mathbf{x}} + \frac{q_s}{m_s} (\mathbf{E} + \mathbf{v} \times \mathbf{B}) \cdot \frac{\partial f_s}{\partial \mathbf{v}} = \left. \frac{\partial f_s}{\partial t} \right|_{collisions} \quad (1)$$

for each species s, e.g. ions, electrons, neutrals. Combined with Maxwell's equations, the system leads to the *continuum kinetic plasma model*, as well as the particle kinetic plasma model. Kinetic models, in their most general form, are six-dimensional, but reduced models with limited dimensionality can also be meaningful, e.g. gyrokinetic. Further reduced plasma models result by taking moments over velocity space of Eq. (1) and of f_s, which gives the *multi-fluid plasma model*. [1]

The principal variables for each species of the multi-fluid plasma model are derived by computing moments of the distribution functions.

$$\rho_s = m_s \int f_s(\mathbf{v}) d\mathbf{v} \quad (2)$$

$$\rho_s \mathbf{u}_s = m_s \int \mathbf{v} f_s(\mathbf{v}) d\mathbf{v} \quad (3)$$

$$\mathbf{P}_s = m_s \int \mathbf{w}\mathbf{w} f_s(\mathbf{v}) d\mathbf{v} \quad (4)$$

$$\mathbf{H}_s = m_s \int \mathbf{w}\mathbf{w}\mathbf{w} f_s(\mathbf{v}) d\mathbf{v} \quad (5)$$

The 5*M* model directly evolves the variables given by Eqs. (2,3) and the tensor contraction of Eq. (4),

$$p_s = \rho_s T_s = \frac{1}{3} m_s \int w^2 f_s(\mathbf{v}) d\mathbf{v}, \quad (6)$$

where T_s is the temperature. The 13*M* model [2] directly evolves the variables given by Eqs. (2,3,4), and the tensor contraction of Eq. (5),

$$\mathbf{h}_s = \frac{1}{2} m_s \int w^2 \mathbf{w} f_s(\mathbf{v}) d\mathbf{v} \quad (7)$$

The system of moment equations is truncated, retaining only variables with a physical meaning. Higher moment variables that appear in the evolution equation are related to lower moment variables.

The multiple fluids are coupled to each other and to the electromagnetic fields through Maxwell's equations and interaction source terms, such as the Lorentz force. Including elastic scattering and reacting collisions (e.g. ionization, recombination, charge exchange) introduces additional source terms that

*This work is supported by a grant from the U.S. Air Force Office of Scientific Research.

978-1-4673-5168-3/13/$31.00 ©2013 IEEE

TABLE I. TYPICAL TIME SCALES (IN SECONDS) FOR LABORATORY AND IONOSPHERIC PLASMAS SHOWING THE LARGE SEPARATION.

	Laboratory FRC	Ionosphere F Region
$1/\omega_{pe}$	5×10^{-14}	6×10^{-8}
L/c	3×10^{-9}	7×10^{-2}
$1/\omega_{ci}$	10^{-8}	4×10^{-3}
L/v_A	10^{-5}	3×10^{1}
L/v_{Ti}	4×10^{-5}	10^{4}
τ_{eq}	10^{-3}	10^{5}

couple the fluids. For example, the governing equations for the electron fluid for an interacting three-fluid model (electron, ion, neutral) is given by

$$\frac{\partial \rho_e}{\partial t} + \nabla \cdot (\rho_e \mathbf{u}_e) = m_e \Gamma_i^{ion} - m_e \Gamma_n^{rec} \tag{8}$$

$$\begin{aligned} \frac{\partial \rho_e \mathbf{u}_e}{\partial t} + \nabla \cdot (\rho_e \mathbf{u}_e \mathbf{u}_e + p_e \mathbf{I} + \Pi_e) &= -\mathbf{R}_i^{ie} + \mathbf{R}_e^{en} \\ - \frac{\rho_e e}{m_e} (\mathbf{E} + \mathbf{u}_e \times \mathbf{B}) + m_e \mathbf{u}_n \Gamma_i^{ion} &- m_e \mathbf{u}_e \Gamma_n^{rec} \end{aligned} \tag{9}$$

$$\begin{aligned} \frac{\partial \varepsilon_e}{\partial t} + \nabla \cdot (((\varepsilon_e + p_e)\mathbf{I} + \Pi_e) \cdot \mathbf{u}_e + \mathbf{h}_e) &= Q_e^{ie} + Q_e^{en} \\ -Q_e^{rec} + \frac{m_e}{m_n} Q_n^{ion} - \mathbf{u}_e \cdot \left(\frac{\rho_e e}{m_e} \mathbf{E} + \mathbf{R}_i^{ie} - \mathbf{R}_e^{en} \right) & \\ -\frac{1}{2} m_e v_e^2 \Gamma_n^{rec} + \left(\frac{1}{2} m_e v_n^2 - \phi_{ion} \right) \Gamma_i^{ion} & \end{aligned} \tag{10}$$

where the source and sink rates are computed by the appropriate convolution integrals, such as the ion source rate from electron impact ionization with neutrals

$$\Gamma_i^{ion} = \int f_n(\mathbf{v}') \int f_e(\mathbf{v}) \sigma_{ion} \left(|\mathbf{v} - \mathbf{v}'| \right) |\mathbf{v} - \mathbf{v}'| \, d\mathbf{v} d\mathbf{v}'. \tag{11}$$

See Ref. [3] for the details of the 5*M* multi-fluid plasma model. Additional moment models can be found in Refs. [4]–[7].

The governing equations for the 5*M* or 13*M* model can be expressed in balance law form as

$$\frac{\partial}{\partial t} q + \nabla \cdot F = S, \tag{12}$$

where q is the vector of conserved variables, F is the flux tensor, and S is vector of source terms. Combining the fluid eigenvalues computed from the flux Jacobian ($\partial F / \partial Q$) with the characteristics of Maxwell's equations and of the source terms provides the characteristic speeds and frequencies, and thereby the time scales given by the plasma model. Table I shows typical values for a laboratory FRC plasma and an ionospheric plasma in the F region. The large separation of the physical time scales makes the equation system mathematically stiff, which can complicate an accurate numerical solution.

III. FINITE ELEMENT METHODS

Finite element (FE) methods offer high-order spatial accuracy in an unsplit approach that tightly couples the flux and source terms in Eq. (12). High-order accurate FE methods are appropriate for problems that have strong anisotropies, complicated geometries, or stiff governing equations. Magnetized plasma simulations of realistic devices using the continuum kinetic or the multi-fluid plasma models are examples that benefit from high-order accuracy. The general approach of FE methods expands the solution vector using a set of basis functions, $v_k(\mathbf{r})$.

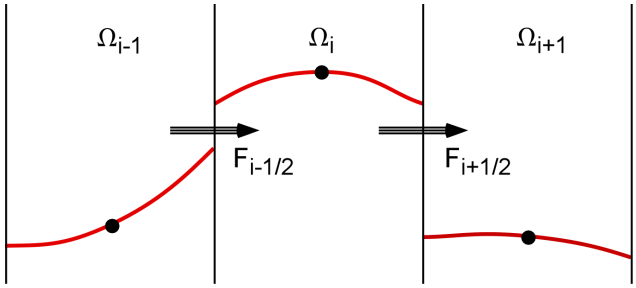

Fig. 1. Schematic representation of a discontinuous, high-order solution within each element Ω having continuous fluxes.

$$q(\mathbf{r}) = \sum_k q_k v_k(\mathbf{r}) \tag{13}$$

The governing equation is then projected onto test functions using a Galerkin method as

$$\int_\Omega v_k \frac{\partial q}{\partial t} dV + \int_\Omega v_k \nabla \cdot \mathbf{F} dV = \int_\Omega v_k S dV \tag{14}$$

where an integral equation is generated for each basis (test) function. Integrating by parts and applying the divergence theorem gives

$$\int_\Omega v_k \frac{\partial q}{\partial t} dV + \oint_{\partial\Omega} v_k \mathbf{F} \cdot d\mathbf{S} - \int_\Omega \mathbf{F} \cdot \nabla v_k dV = \int_\Omega v_k S dV \tag{15}$$

This equation is valid in general but is inconvenient for realistic domains with complicated geometries. Instead, the domain is divided into finite elements, and the integral equation is applied to each element with some assumption of continuity at the element boundaries.

If the solution is assumed to be continuous (C^0), the fluxes are automatically continuous, and the result is the usual finite element method. During assembly of the global system for the simultaneous solution for all q_k^Ω, the surface integral term in Eq. (15) cancels everywhere except at the domain boundaries. Volume integrals are evaluated by quadrature. The continuous FE method works well for many elliptic and parabolic systems on complicated geometries; however, spurious oscillations can occur at discontinuities (shocks) for hyperbolic systems, which means the method is not suitable for many plasma simulations.

If the solution is allowed to be discontinuous, but with continuous fluxes, which is the only feature required by the conservation law, the resulting finite element system is the discontinuous Galerkin (DG) method. [8], [9] See Fig. 1 for a schematic representation of the DG method. Fluxes in the surface integral term in Eq. (15) are evaluated using an upwind method such as an approximate Riemann solver [4], [10] with solution values on either side of the interface.

$$\mathbf{F}_{\partial\Omega} = \frac{1}{2} \left(\mathbf{F}^+ + \mathbf{F}^- \right) - \frac{1}{2} \sum_k l_k \left(q^+ - q^- \right) |\lambda_k| \, r_k \tag{16}$$

Limiting is accomplished by locally reducing the expansion order. Time is advanced using a Runge-Kutta method, for example the third-order, TVD method. [11]

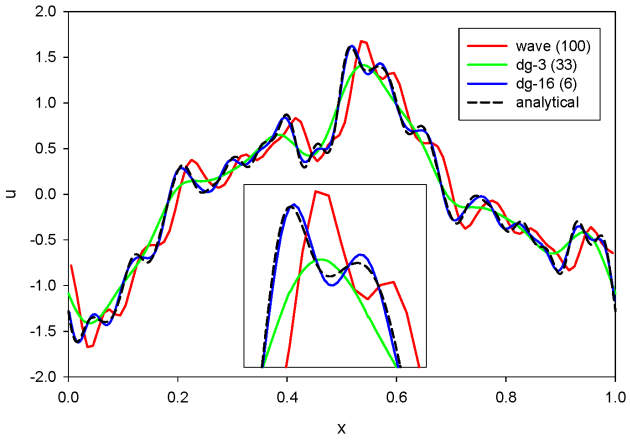

Fig. 2. Evolved solutions for the electrostatic ion cyclotron waves with different orders of accuracy with approximately equivalent effective resolution: 2^{nd} order finite volume method with 100 cells, 3^{rd} order DG method with 33 elements, 16^{th} order DG method with 6 elements, and the analytical solution. The inset shows the details around the highest peak.

The DG method has been implemented in a flexible code framework, WARPX (Washington Approximate Riemann Plasma code), that simplifies extension of the physical model. [1] Exercising the DG method within WARPX has been successful for modeling plasma phenomena using the two-fluid and MHD plasma models. [9], [12]–[15] The code runs on multi-processor machines using MPI and on many-core and GPU systems using OpenCL. The algorithm is applicable to study advanced physics calculations of plasma dynamics including HEDP, magnetic plasma confinement, and astrophysical plasmas.

IV. Numerical Results

A motivation for high-order accuracy is the unsplit coupling of the hyperbolic fluxes and the source terms represented in Eq. (12). The benefits are demonstrated by the propagation of electrostatic ion cyclotron waves and by equilibrium calculations. [14] The electrostatic ion cyclotron waves are highly dispersive with an analytical solution given by

$$u_x(x,t) = -\sum_{n=0}^{\infty} \frac{u^0}{2n+1} \sin\left(k_n x + \omega_n t\right) \qquad (17)$$

where $\omega_n^2 = k_n^2 c_s^2 + \omega_c^2$ and u^0 is the initial wave amplitude. The solution is computed using the DG method in WARPX with different orders of basis functions but maintaining approximately equivalent effective resolution, i.e. the number of unknowns is constant, 2^{nd} order finite volume method with 100 cells, 3^{rd} order DG method with 33 elements, and 16^{th} order DG method with 6 elements. The results are shown in Fig. 2. Higher order solutions better match the analytical result with the 16^{th} order solution closely following the analytical solution even with only 6 elements. The discrepancies in the solutions are clearly seen in the inset of Fig. 2.

High-order accuracy is also important for preserving anisotropies, which often occur in plasmas. Plasmas are often strongly magnetized which produces strongly anisotropic transport properties. One example is thermal conductivity can have a ratio of parallel to perpendicular conductivities of 10^6. The effect has been investigated using a high-order finite element method to solve the anisotropic heat conduction equation.

$$\frac{\partial T}{\partial t} + \nabla \cdot (-\mathbf{D} \cdot \nabla T) = 0 \qquad (18)$$

where $\mathbf{D} = \mathbf{D}_{||}(x,y,z) + \mathbf{D}_{\perp}(x,y,z)$. The problem is initialized in 3D with a Gaussian temperature profile aligned with a toroidal magnetic field. The diffusivities are set with $\mathbf{D}_{||} = 1$ and $\mathbf{D}_{\perp} = 0$. Numerical solutions are found for varying number of elements and for varying order of the basis functions. The numerical solutions are analyzed to determine an effective $\mathbf{D}_{\perp}$. Results show the expected behavior of decreasing $\mathbf{D}_{\perp}$ as spatial resolution is increased with either smaller elements or higher order basis functions. Even for equivalent effective resolutions, higher order is better able to preserve anisotropy. Details of this investigation are described in Ref. [16].

The DG method has been applied to solve the Vlasov-Poisson kinetic model (collisionless Boltzmann) to demonstrate accurate, validated results. The solution of the continuum kinetic model has been benchmarked to weak and strong Landau damping and to the two-stream instability of Cheng and Knorr. [17] Figure 3 shows the simulation results at a normalized time of $\omega_p t = 60$. The simulation uses a grid of 20×80 elements using 7^{th} order polynomials in (x, v_x). Note the high-order representation accurately captures the striations the occur in phase space as the solution develops.

Since the advanced plasma models solved in the approach described above are coupled to Maxwell's equations, fast waves may propagate to domain boundaries and cause unphysical reflections. The fast waves are also indicated in Table I. Several techniques have been developed to address wave interactions with the boundary. The Calderon projection technique exhibits high accuracy without increasing the domain size. [18] This method is particularly useful when external magnetic fields are applied that vary slowly compared to the plasma dynamics.

To treat open boundaries without generating non-physical reflections, non-local boundary conditions must be employed. Simpler methods work for normal incidence waves, but waves with oblique incidence can be problematic. Lacuna-based methods append an auxiliary domain and replace the open boundary with an interface matching condition. For the mathematical details and a thorough review of the method, see Ref. [19]. The solutions between the interior domain and the auxiliary domain are smoothed with a transition function. See Fig. 4 for an illustration of the domains. Waves propagate out of the interior domain without reflecting or returning.

The governing equation in the interior domain is expressed as given by Eq. (12), while in the auxiliary domain the governing equation is defined as

$$\frac{\partial w}{\partial t} + \nabla \cdot \mathbf{F}(w) = S(w) + \Omega(q) \qquad (19)$$

where $w = \mu q$ and $\mu = \mu(x)$ is the transition function, again see Fig. 4. The "transition region" source term $\Omega(q)$ is determined to guarantee that the interior solution matches the exterior solution at the interface. Namely,

$$\Omega(q) = \nabla \cdot \mathbf{F}(\mu q) - S(\mu q) - \mu \nabla \cdot \mathbf{F}(q) + \mu S(q) \qquad (20)$$

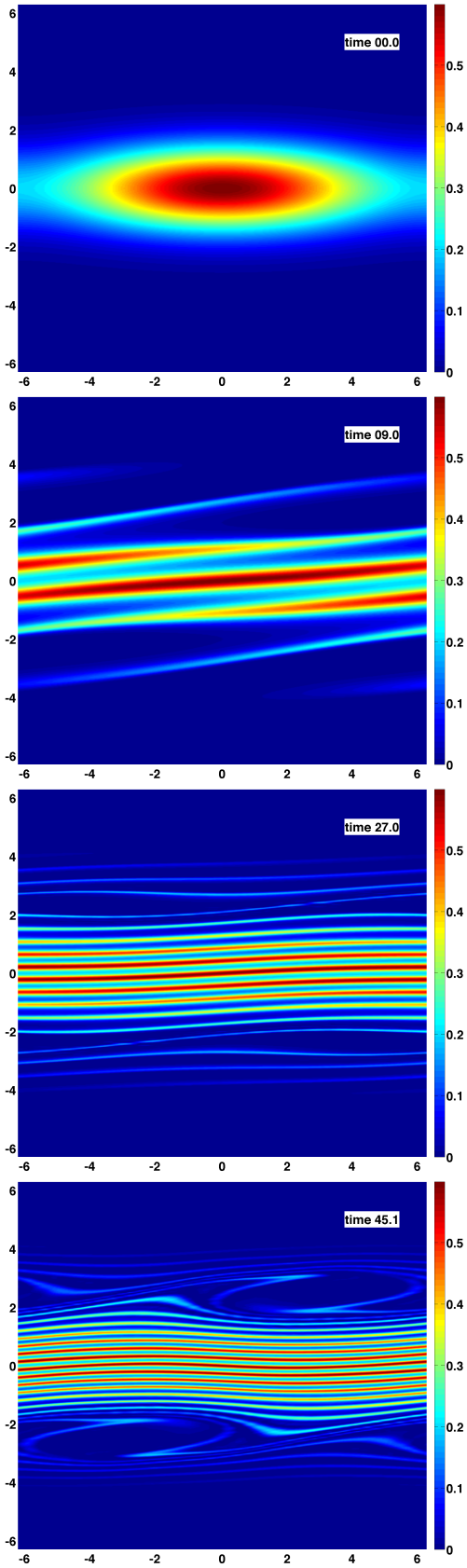

Fig. 3. Evolution of the strong Landau damping using 7^{th} order discontinuous FE representation which accurately captures the fine-scale striations that develop in phase space.

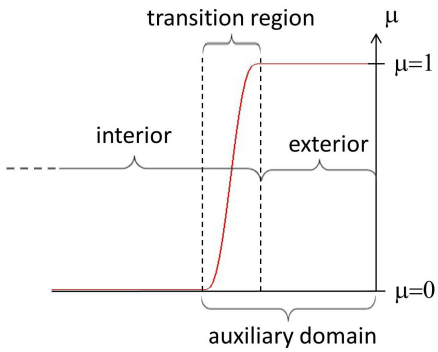

Fig. 4. Illustration for the lacuna-based boundary conditions. The original (interior) domain is appended with an overlapping auxiliary domain that transmits waves without reflections.

The boundary condition for the interior solution q is set such that

$$q|^{-}_{interface} = w|^{+}_{interface} \tag{21}$$

The auxiliary solution is periodically re-integrated to damp the solution before it reflects and contaminates the solution at the interface.

Lacuna-based methods work for oblique incidence waves in either purely hyperbolic or mixed hyperbolic/parabolic systems. [20] The method even works in 2D where no true lacunae exist. (Huygens' principle states true lacunae only exist in odd dimensional space.) The performance is demonstrated in the numerical results shown in Fig. 5. The cylindrical propagation of an electromagnetic wave intersects open boundaries on the lower and left edges of the domain. The figure shows the combined interior and exterior domains on the left and only the interior domain on the right. The wave smoothly exits the interior domain and decays before interacting with the boundary of the exterior domain. No artificial reflections are generated even from the wave that is incident oblique to the boundary.

V. Conclusions

Plasmas are accurately described with continuum models: from detailed kinetic models to 5*M* and 13*M* moment models. This paper highlights developments in high-order techniques for solving these systems of equations so as to create high-fidelity methods that are better able to capture complex plasma physics phenomena. Coupling these models to high-order spatial representations leads to numerical algorithms that capture appropriate physical phenomena. High-order accuracy is important to capture the delicate balance of fluxes and sources in advanced plasma models and the large anisotropic character in magnetized plasmas. The discontinuous Galerkin FE method has been implemented into the WARPX code and has been validated to analytical results and benchmarked to published computational results.

References

[1] U. Shumlak, R. Lilly, N. Reddell, E. Sousa, and B. Srinivasan. Advanced physics calculations using a multi-fluid plasma model. *Computer Physics Communications*, 182(9):1767 – 1770, 2011.

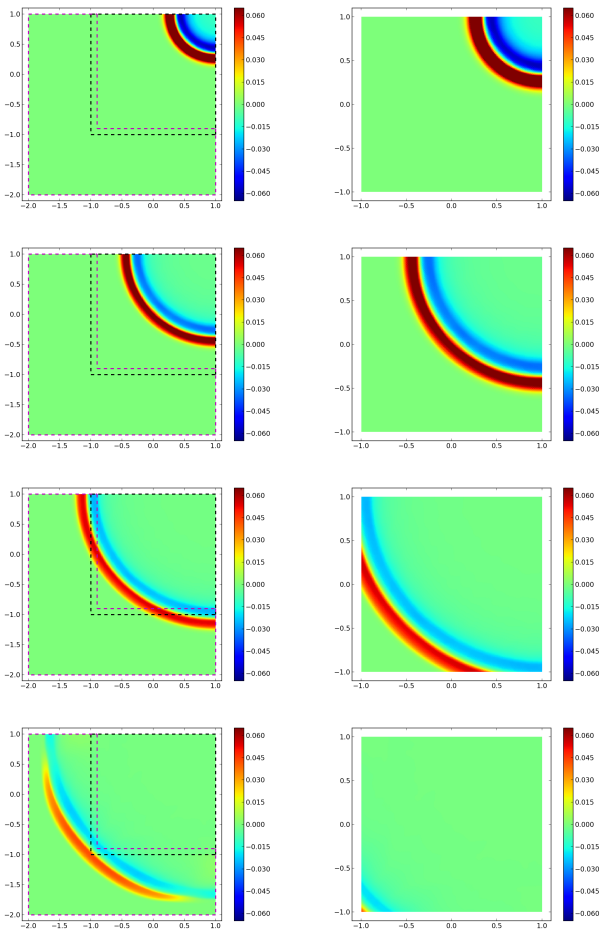

Fig. 5. Cylindrical propagation of an electromagnetic wave intersecting open boundaries on the lower and left edges of the domain. Left shows the interior and exterior domains with dashed lines indicating the transition region. Right shows only the interior domain revealing no trace of reflected waves.

[2] H Grad. On The Kinetic Theory Of Rarefied Gases. *Communications On Pure And Applied Mathematics*, 2(4):331–407, 1949.

[3] E. T. Meier and U. Shumlak. A general nonlinear fluid model for reacting plasma-neutral mixtures. *Physics of Plasmas*, 19(7):072508, 2012.

[4] U. Shumlak and J. Loverich. Approximate Riemann solver for the two-fluid plasma model. *Journal of Computational Physics*, 187(2):620 – 638, 2003.

[5] A. Hakim and U. Shumlak. Two-fluid physics and field-reversed configurations. *Physics of Plasmas*, 14(5):055911, 2007.

[6] Manuel Torrilhon. Hyperbolic Moment Equations in Kinetic Gas Theory Based on Multi-Variate Pearson-IV-Distributions. *Communications in Computational Physics*, 7(4):639–673, Apr 2010.

[7] S. Gilliam. A 13-moment two-fluid plasma physics model based on a Pearson type-IV distribution function. Master's thesis, University of Washington, Seattle, WA 98195, September 2011.

[8] B Cockburn and CW Shu. TVB Runge-Kutta Local Projection Discontinuous Galerkin Finite-Element Method For Conservation-Laws. *Mathematics Of Computation*, 52(186):411–435, 1989.

[9] J. Loverich, A. Hakim, and U. Shumlak. A discontinuous Galerkin method for ideal two-fluid plasma equations. *Communications in Computational Physics*, 9:240–268, 2011.

[10] P. L. Roe. Approximate riemann solvers, parameter vectors and difference schemes. *Journal of Computational Physics*, 43:357, 1981.

[11] B Cockburn and CW Shu. Runge-Kutta Discontinuous Galerkin Methods for Convection-Dominated Problems. *Journal of Scientific Computing*, 16(3):173–261, Sep 01 2001.

[12] J. Loverich and U. Shumlak. A discontinuous Galerkin method for the full two-fluid plasma model. *Computer Physics Communications*, 169(1-3):251 – 255, 2005.

[13] J. Loverich and U. Shumlak. Nonlinear full two-fluid study of $m = 0$ sausage instabilities in an axisymmetric Z pinch. *Physics of Plasmas*, 13(8):082310, 2006.

[14] B. Srinivasan, A. Hakim, and U. Shumlak. Numerical methods for two-fluid dispersive fast MHD phenomena. *Communications in Computational Physics*, 10:183–215, Mar 2011.

[15] B. Srinivasan and U. Shumlak. Analytical and computational study of the ideal full two-fluid plasma model and asymptotic approximations for hall-magnetohydrodynamics. *Physics of Plasmas*, 18(9):092113, 2011.

[16] E. T. Meier, V. S. Lukin, and U. Shumlak. Spectral element spatial discretization error in solving highly anisotropic heat conduction equation. *Computer Physics Communications*, 181(5):837–841, May 2010.

[17] C. Z. Cheng and Georg Knorr. The Integration of the Vlasov Equation in Configuration Space. *Journal of Computational Physics*, 22(3):330 – 351, 1976.

[18] E. Kansa, U. Shumlak, and S. Tsynkov. Discrete Calderon's Projections on Parallelepipeds and their Application to Computing Exterior Magnetic Fields for FRC Plasmas. *Journal of Computational Physics*, 234(0):172–198, 2012.

[19] S.V. Tsynkov. On the application of lacunae-based methods to maxwell's equations. *Journal of Computational Physics*, 199(1):126 – 149, 2004.

[20] E.T. Meier, A.H. Glasser, V.S. Lukin, and U. Shumlak. Modeling open boundaries in dissipative mhd simulation. *Journal of Computational Physics*, 231(7):2963 – 2976, 2012.